AIAA JOURNAL
Vol. 38, No. 9, September 2000

Nonlinear Response of Airfoil Section with Control Surface Freeplay to Gust Loads

Deman Tang,* Denis Kholodar,† and Earl H. Dowell‡
Duke University, Durham, North Carolina 27708-0300

A nonlinear response analysis of a typical airfoil section with control surface freeplay excited by periodic gust loads in low subsonic flow is presented along with a companion wind-tunnel test program. The analytical model uses Peters's finite state model for the two-dimensional aerodynamic flow over the airfoil (Peters, D. A., "Finite-State Airloads for Deformable Airfoils on Fixed and Rotating Wings," Symposium on Aeroelasticity and Fluid/Structure Interaction, American Society of Mechanical Engineers, Winter Annual Meeting, Nov. 1994, rev. 3, May 1996). Results for a single harmonic gust and a continuous frequency sweep gust have been computed and measured for flow velocities below the flutter speed. A theoretical and experimental chaotic response phenomenon for the nonlinear structural model was observed. These results further confirm some conclusions about limit cycle oscillations and complement our earlier theoretical and experimental studies of self-excited oscillations. The experimental investigation has been carried out in the Duke University wind tunnel using a rotating slotted cylinder gust generator. The fair to good quantitative agreement between theory and experiment verifies that the present analytical approach has reasonable accuracy and good computational efficiency for nonlinear gust response analysis in the time domain.

Nomenclature

b	= semichord of the airfoil section
c	= position of flap hinge
h	= plunge displacement
L_n	= generalized airloads
M_r	= reference mass/length of wing-aileron system
M_α	= torsional moment about the midchord
M_β	= flap moment about the flap axis
N	= number of inflow states
n	= inflow expansion index
p	= aerodynamic pressure
q	= aerodynamic modal coordinate
t	= time
U	= airspeed
U_f	= flutter airspeed
v	= induced flow normal to airfoil due to bound vorticity
$w_g(x, t)$	= lateral gust velocity
w_{gn}	= expansion coefficients of $w_g(x, t)$
$\bar{w}_{gs}$	= amplitude of sinusoidal gust
x	= streamwise coordinate
y	= coordinate normal to x, lift direction
α	= torsional angle of wing
β	= flap rotational angle
Γ	= vortex strength
γ_b	= bound vorticity
δ	= freeplay region
λ	= induced flow due to free vorticity
λ_n	= expansion coefficients for λ
ξ	= dummy integration variable for x
ρ	= air density
τ_n	= expansion coefficients for $\Delta p/\rho$
ϕ	= Glauert variable
ϕ_m	= location of hinge, $\cos^{-1}(c)$
ω_h, ω_α	= uncoupled plunge and torsional natural frequencies
ω_β	= uncoupled flap natural frequency
$(\dot{})$	= $\mathrm{d}(\,)/\mathrm{d}t$

Received 1 July 1999; revision received 8 December 1999; accepted for publication 10 December 1999.

*Research Associate, Department of Mechanical Engineering and Materials Science.
†Research Assistant, Department of Mechanical Engineering and Materials Science.
‡J. A. Jones Professor and Dean of the School of Engineering.

Introduction

REFERENCE 1 deals with the effect of control surface freeplay on the self-excited aeroelastic response of a three-degree-of-freedom typical airfoil section. The theoretical model was based on the state-space model used by Conner et al.[1] and proposed by Edwards et al.[2] Because the freeplay nonlinearity produces a piecewise linear change in the structural stiffness of the control surface, the overall system can be represented as a nonlinear combination of a three linear system. The response is determined via numerical integration, updating the equations of motion as the system moves from one linear region into the next. Following the work of Ref. 1, we subsequently used Peters's finite state airloads model[3] for the two-dimensional aerodynamic flow over the airfoil to determine the eigenmodes of the aerodynamic flow and then chose a small number of these aerodynamic eigenmodes, that is, reduced-order model, to couple them to a typical section nonlinear structural model.[4] All predicted results from both Refs. 1 and 4 were compared with wind-tunnel test data and showed good agreement. Also the results are consistent with those given in Ref. 5.

Reference 6 describes the military specification that defines the maximum value of freeplay for control surfaces and tabs throughout the life of the airplane. For an all-movable control surface, the total peak-to-peak freeplay gap shall not exceed 0.034 deg, and with this value catastrophic aeroelastic instabilities shall not occur in a velocity range up to 1.15 times the design limit speed of the aircraft. However, freeplay may also modify response to external excitations, and thus study of gust response of an aircraft with a freeplay control surface to atmospheric turbulence is of interest and is the subject of the present paper.

A few years ago, a rotating slotted cylinder (RSC) gust generator was installed in the Duke University low-speed wind tunnel and used to generate a gust excitation field including either a sinusoidal gust or a linear frequency sweep gust excitation.[6] This apparatus provides a tool to assess the accuracy of theoretical methods for determining response to gust loads.

In the present paper, a time-domain method proposed in Ref. 4 is extended to calculate and measure nonlinear gust response when the time-correlated gust loads are known. Of course, the Peters's finite state airloads model[3] considers the effect of gust loads on the aerodynamics as well as the motion induced aerodynamics. Sinusoidal and linear frequency sweep gust loads are used. To validate the theoretically predicted gust response characteristics of the nonlinear aeroelastic system, an experimental investigation has been carried out in the Duke University wind tunnel using an RSC gust generator. The results may be helpful in better understanding physically

the nonlinear aeroelastic response of a typical airfoil section with control surface freeplay to gust loads.

Aerodynamic Theory

We use Peters's finite state incompressible airloads model for a deformable airfoil[3] to determine these aerodynamic forces.

We consider a thin airfoil to be in a moving two-dimensional coordinate system (x–y plane) and to be performing small motion $h(x, t)$ in the y direction and in the interval $-b \le x \le b$, as shown in Fig. 1. The nonpenetration boundary condition on the moving airfoil can be written as

$$v = U\frac{\partial h}{\partial x} + \frac{\partial h}{\partial t} + w_g(t) - \lambda \tag{1}$$

where v is the necessary induced flow in the negative y direction due to bound vorticity, λ is the downwash due to all induced flow, and $w_g(t)$ is a known lateral gust velocity time history (see the next section).

The relationship between the v and the unknown bound vorticity γ_b is given as

$$v = \frac{-1}{2\pi}\int_{-b}^{b}\frac{\gamma_b(\xi, t)}{x-\xi}\,\mathrm{d}\xi \tag{2}$$

and the pressure difference across the airfoil is

$$\Delta p = \rho U\gamma_b + \rho\int_{-b}^{x}\frac{\partial\gamma_b}{\partial t}\,\mathrm{d}\xi \tag{3}$$

For the two-dimensional case of Fig. 1, the induced flow λ due to free vorticity is given by

$$\frac{\partial\lambda}{\partial t} + U\frac{\partial\lambda}{\partial x} = \frac{1}{2\pi}\frac{\partial\Gamma/\partial t}{b-x} \tag{4}$$

where Γ is the total bound vorticity on the airfoil,

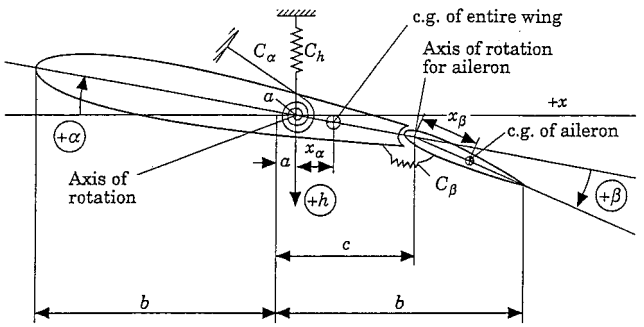

Fig. 1a Aeroelastic typical section with control surface.

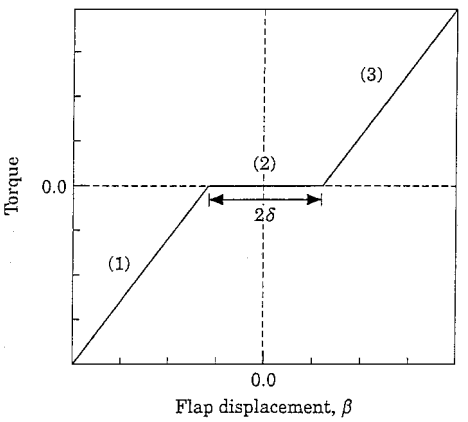

Fig. 1b Restoring moment due to K_β with a symmetric freeplay region about $\beta = 0$.

$$\Gamma \equiv \int_{-b}^{b}\gamma_b\,\mathrm{d}x \tag{5}$$

By the use of a Glauert variable ϕ, then

$$x = b\cos\phi, \qquad -b \le x \le b, \quad 0 \le \phi \le \pi \tag{6}$$

The appropriate expansions follow from thin-airfoil theory:

$$\gamma_b = 2\left[\frac{\gamma_s}{\sin\phi} - \frac{\gamma_0\cos\phi}{\sin\phi} + \sum_{n=1}^{\infty}\gamma_n\sin(n\phi)\right] \tag{7}$$

$$\Delta p = 2\rho\left[\frac{\tau_s}{\sin\phi} - \frac{\tau_0\cos\phi}{\sin\phi} + \sum_{n=1}^{\infty}\tau_n\sin(n\phi)\right] \tag{8}$$

Following Eqs. (2), (7), and (8), we have

$$v = \sum_{n=0}^{\infty}\gamma_n\cos(n\phi) \tag{9}$$

$$\lambda = \sum_{n=0}^{\infty}\lambda_n\cos(n\phi) \tag{10}$$

$$h = \sum_{n=0}^{\infty}h_n\cos(n\phi) \tag{11}$$

and the lateral gust velocity is expanded as follows:

$$w_g = \sum_{n=0}^{\infty}w_{gn}\cos(n\phi) \tag{12}$$

From the preceding equations, generalized forces associated with each generalized airfoil motion h_n and the generalized gust loads w_{gn} can be obtained. They are

$$L_n = -\int_{-b}^{b}\Delta p\cos(n\phi)\,\mathrm{d}x = -\int_{0}^{\pi}b\Delta p\cos(n\phi)\sin\phi\,\mathrm{d}\phi \tag{13}$$

Using the Kutta condition of $\Delta p = 0$ at the trailing edge and the substitution of Eq. (8) into Eq. (13), we then have for L_0 (lift per unit length normalized on semichord b)

$$L_0 = -2\pi\rho U(w_0 - \lambda_0) - \pi\rho U w_1 - \pi\rho b\left(\dot{w}_0 - \tfrac{1}{2}\dot{w}_2\right) \tag{14}$$

for L_1 (pitching moment per unit length about midchord)

$$L_1 = \pi\rho U(w_0 - \lambda_0) - \tfrac{1}{2}\pi\rho U w_2 - \tfrac{1}{8}\pi\rho b(\dot{w}_1 - \dot{w}_3) \tag{15}$$

and for L_2

$$L_2 = \tfrac{1}{2}\pi\rho U(w_1 - w_3) + \tfrac{1}{2}\pi\rho b\left(\dot{w}_0 - \tfrac{1}{2}\dot{w}_2\right) - \tfrac{1}{12}\pi\rho b(\dot{w}_2 - \dot{w}_4) \tag{16}$$

For $n \ge 3$,

$$L_n = \tfrac{1}{2}\pi\rho U(w_{n-1} - w_{n+1}) + [1/4(n-1)]\pi\rho b(\dot{w}_{n-2} - \dot{w}_n) - [1/4(n+1)]\pi\rho b(\dot{w}_n - \dot{w}_{n+2}) \tag{17}$$

where

$$w_0 = w_{g0} + \dot{h}_0 + U\sum_{n=1,3,5}^{\infty}\frac{nh_n}{b}$$

$$w_1 = w_{g1} + \dot{h}_1 + 2U\sum_{n=2,4,6}^{\infty}\frac{nh_n}{b}$$

$$w_m = w_{gm} + \dot{h}_m + 2U\sum_{n=m+1,m+3}^{\infty}\frac{nh_n}{b}, \qquad m \ge 2$$

Substituting Eq. (10) into Eq. (4), we obtain a set of differential equations for the λ_n coefficients:

$$b\left(\dot{\lambda}_0 - \tfrac{1}{2}\dot{\lambda}_2\right) + U\lambda_1 = \dot{\Gamma}/\pi$$

$$(b/2n)(\dot{\lambda}_{n-1} - \dot{\lambda}_{n+1}) + U\lambda_n = \dot{\Gamma}/(n\pi), \qquad n \geq 2 \quad (18)$$

where

$$\Gamma = 2\pi b\left[w_{g0} + \dot{h}_0 - \lambda_0 + \frac{1}{2}(w_{g1} + \dot{h}_1 - \lambda_1) + U\sum_{n=1}^{\infty}\frac{nh_n}{b}\right]$$

Gust Loads

Atmospheric turbulence creates a gust load that can be represented by two different mathematical descriptions. One is associated with a discrete gust representation usually of a deterministic nature. Continuous turbulence, however, can be represented by a stochastic process. In the present work, a discrete gust representation is required.

In general, atmospheric turbulence is considered to be a function of three spatial dimensions and time. In this paper, the atmospheric turbulence velocity field is composed of only a lateral component, and the frozen gust assumption is used.[7] For the frozen gust, x and t are coordinates fixed with respect to airfoil and x' and t' are coordinates fixed with respect to atmosphere. The gust field is given by

$$w_g(x') = w_g(x - Ut)$$

Because x and t only appear in the preceding combination, we may consider the alternative functional form

$$w_g = w_g(t - x/U)$$

We assume that, at $t = t_0$, the leading edge of the airfoil has a gust velocity

$$w_{gl} = w_g(t_0 + b/U) \qquad (x = -b)$$

and at the trailing edge of the airfoil, the gust velocity is

$$w_{gt} = w_g(t_0 - b/U) \qquad (x = b)$$

If the gust is known as a discrete time series with a constant sampling time step length Δt, the gust at any chordwise position of the airfoil, x_j, is

$$w_{gc}(t_0) = w_g(t_0 + x_j/U) = w_g(t_0 + j\Delta t) \quad (19)$$

where j is an integral number starting from the leading edge, $j = 1$, and ending at the trailing edge, $j = n_s$, where $n_s = 2b/U\Delta t$.

At $t = t_0$, the w_{gn} coefficients of Eq. (12) can be determined by

$$w_{g0}(t_0) = \frac{1}{\pi}\int_0^{\pi} w_{gc}(t_0, x)\,\mathrm{d}\phi = \frac{1}{\pi}\int_{-b}^{b}\frac{w_{gc}(t_0)}{b\sin[(\cos^{-1}(x/b)]}\,\mathrm{d}x$$

$$= \frac{1}{b\pi}\sum_{j=1}^{n_s}\frac{w_{gc}(t_0, x_j)\Delta x}{\sin(\cos^{-1}\phi_j)} \quad (20)$$

where $\phi = \cos^{-1}(x/b)$, and $\Delta x = U\Delta t$, $x_j = j\Delta x$, and $\phi_j = (x_j - b)/b$,

$$w_{gn}(t_0) = \frac{2}{\pi}\int_0^{\pi} w_{gc}(t_0, x)\cos n\phi\,\mathrm{d}\phi$$

$$= \frac{2}{b\pi}\sum_{j=1}^{n_s}\frac{w_{gc}(t_0, x_j)\cos\left(n\cos^{-1}\phi_j\right)\Delta x}{\sin\left(\cos^{-1}\phi_j\right)} \quad (21)$$

Thus, $w_{g0}(t_0)$ and $w_{gn}(t_0)$ can be determined using a standard numerical integration code. When we use a time-integral method to solve the nonlinear equations, those coefficients need to be evaluated at each time step.

Two special periodic gusts are used for comparison with our experimental results. One is a continuous sinusoidal gust. It is expressed as

$$w_g(t) = \bar{w}_{gs}\sin\omega t \quad (22)$$

where ω is the gust excitation frequency. The other is a continuous frequency sweep gust, and it is expressed as

$$w_g(t) = \bar{w}_{gs}\sin\{\omega_1 + [(\omega_2 - \omega_1)/2T]t\}t \quad (23)$$

where ω_1, ω_2, and T are the minimum frequency, maximum frequency, and the sweep duration, respectively.

For a sinusoidal gust, the w_{gn} coefficients of Eq. (12) are determined by

$$w_{g0}(t_0) = \frac{1}{\pi}\int_0^{\pi}\bar{w}_{gs}\sin(\omega t - \Delta\psi)\,\mathrm{d}\phi$$

$$= \frac{\bar{w}_{gs}}{b\pi}[C_0\sin\omega t - S_0\cos\omega t] \quad (24)$$

where

$$C_0 = \sum_{j=1}^{n_s}\frac{\cos\Delta\psi\Delta x}{\sin\left(\cos^{-1}\phi_j\right)}, \qquad S_0 = \sum_{j=1}^{n_s}\frac{\sin\Delta\psi\Delta x}{\sin\left(\cos^{-1}\phi_j\right)}$$

and for $n \geq 1$,

$$w_{gn}(t_0) = \frac{2}{\pi}\int_0^{\pi}\bar{w}_{gs}\sin(\omega t - \Delta\psi)\cos n\phi\,\mathrm{d}\phi$$

$$= \frac{2\bar{w}_{gs}}{b\pi}[C_n\sin\omega t - S_n\cos\omega t] \quad (25)$$

where

$$C_n = \sum_{j=1}^{n_s}\frac{\cos\Delta\psi\cos\left(n\cos^{-1}\phi_j\right)\Delta x}{\sin\left(\cos^{-1}\phi_j\right)}$$

$$S_n = \sum_{j=1}^{n_s}\frac{\sin\Delta\psi\cos\left(n\cos^{-1}\phi_j\right)\Delta x}{\sin\left(\cos^{-1}\phi_j\right)}$$

$\Delta\psi$ is a phase difference that is defined as $\Delta\psi = x_j/l_g$, and l_g is the gust wavelength that is defined as $l_g = U/\omega$. Note that the integral terms, C_0, C_n, S_0, and S_n do not need to be evaluated at each time step.

State-Space Equations

A schematic of a typical airfoil section with a control surface at the trailing edge of the main wing is shown in Fig. 1. There is a structural freeplay nonlinearity that produces a piecewise linear change in the structural stiffness of the control surface. The aeroelastic typical section has three degrees of freedom (DOF), plunge h, torsion α of the main wing, and rotation β of the control surface about the point c. For deflection of the flap through an angle β of the rigid-body airfoil, the h_n coefficients of Eq. (11) are

$$h_0 = \frac{1}{\pi}\int_0^{\pi} h\,\mathrm{d}\phi = \frac{1}{\pi}\int_0^{\pi_m}\beta(\cos\phi - \cos\phi_m)bh\,\mathrm{d}\phi$$

$$= \frac{\beta b}{\pi}(\sin\phi_m - \phi_m\cos\phi_m)$$

$$h_1 = \frac{2}{\pi}\int_0^{\pi} h\cos\phi\,\mathrm{d}\phi = \frac{\beta b}{\pi}(\phi_m - \sin\phi_m\cos\phi_m)$$

$$h_n = \frac{2}{\pi}\int_0^{\pi} h\cos(n\phi)\,\mathrm{d}\phi$$

$$h_n = \frac{\beta b}{\pi}\left[\frac{1}{n+1}\sin(n+1)\phi_m + \frac{1}{n-1}\sin(n-1)\phi_m - \frac{2}{n}\sin(n\phi_m)\cos\phi_m\right]$$

where ϕ_m is the Glauert angle at the hinge, $\cos^{-1}(bc)$.

For the special case of a rigid-body airfoil without a control surface in a fixed stream, we have $h_0 = h - ba\alpha$ and $h_1 = b\alpha$. Thus,

a matrix form for the h_n in terms of the airfoil DOF, h, α, and β is

$$\{h_n\} = [T] \begin{Bmatrix} h \\ \alpha \\ \beta \end{Bmatrix} \tag{26}$$

The differential equations of structural motion in matrix form [Eq. (27)] expressing the equilibrium of the moments about point a of the entire airfoil, of the moments on the control surface about point c, and of the vertical forces on the airfoil (see Fig. 1) are as follows:

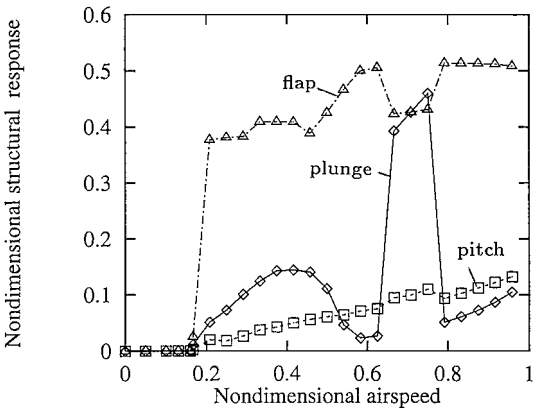

Fig. 2 Nondimensional structural response vs nondimensional airspeed for no gust excitation.

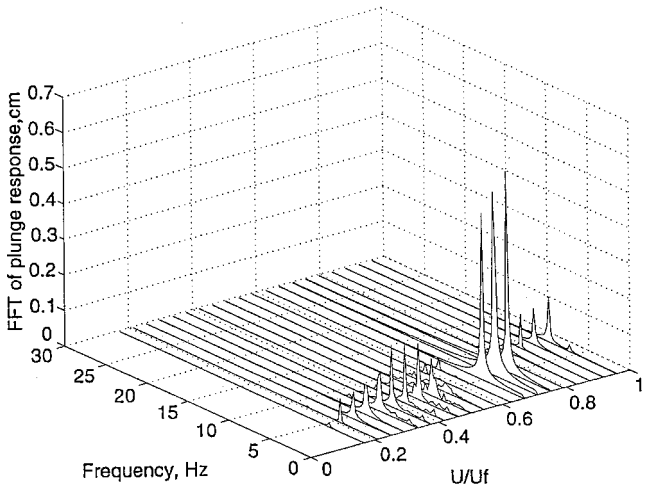

a) Plunge response

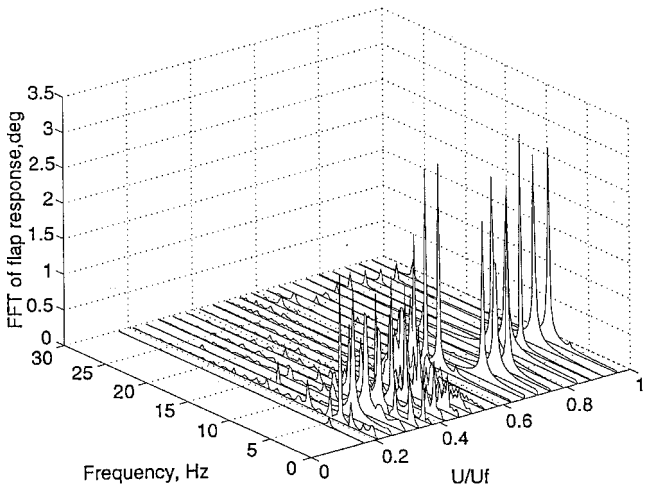

b) Flap response

Fig. 3 FFT analysis vs nondimensional airspeed for no gust excitation.

$$[M_s]\{\ddot{y}\} + [C_s]\{\dot{y}\} + [K_s]\{y\} + \{M_\beta\} = [S_1]\{F_a\} \tag{27}$$

where $\{y\}$ is expressed as $\{h, \alpha, \beta\}^T$, $\{M_\beta\} = \{0, 0, M_\beta\}^T$,

$$[S_1] = \begin{bmatrix} 1/M_r b & 0 & 0 \\ 0 & 1/M_r b^2 & 0 \\ 0 & 0 & 1/M_r b^2 \end{bmatrix}$$

and

$$[K_s] = \begin{bmatrix} K_h & 0 & 0 \\ 0 & K_\alpha & 0 \\ 0 & 0 & \nu K_\beta \end{bmatrix}$$

When the structural freeplay gap δ is zero, then $\nu = 1$ and $M_\beta = 0$, and when the structural freeplay gap is not zero, then $\nu = 0$ and the control surface moment–rotation relationships may be expressed as

$$M_\beta = \begin{cases} K_\beta(\beta - \delta) & |\beta| \geq \delta, \quad \beta > 0 \\ K_\beta(\beta + \delta) & |\beta| \geq \delta, \quad \beta < 0 \\ 0 & \text{otherwise} \end{cases} \tag{28}$$

and $[C_s]$ is the structural damping matrix. An attempt has been made here to include structural damping in the numerical model

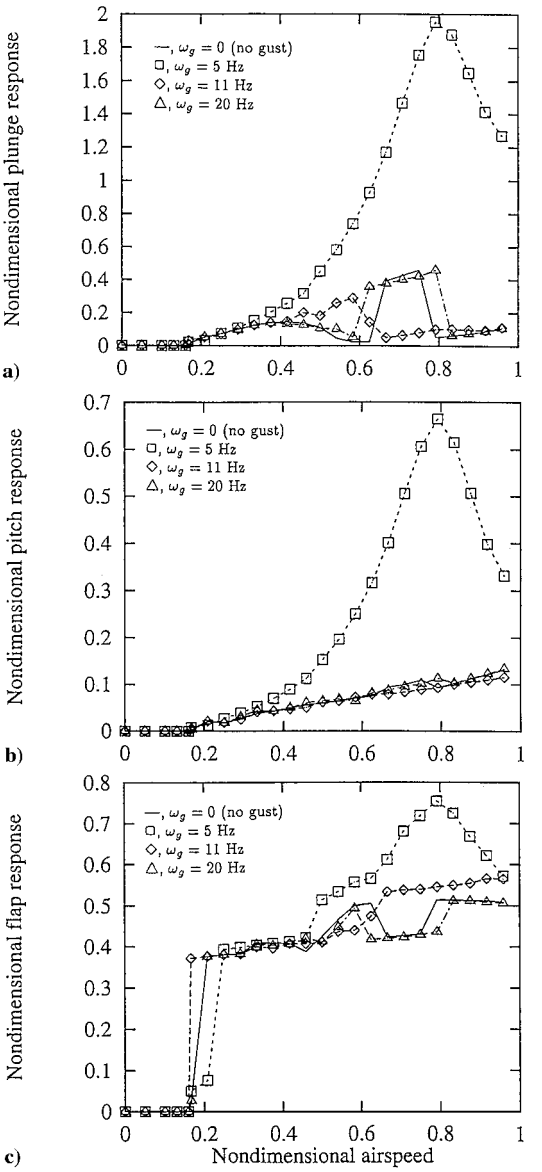

Fig. 4 Nondimensional structural response vs nondimensional airspeed for gust excitation frequencies ω_g = 5, 11, and 20 Hz for a) plunge response, b) pitch response, and c) flap response.

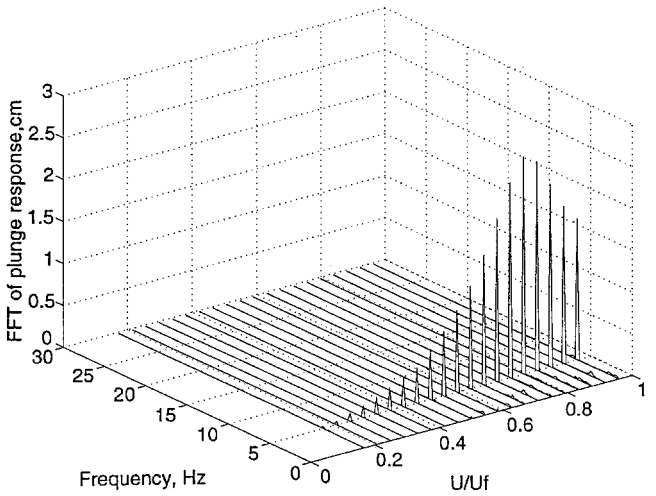

a) Plunge response

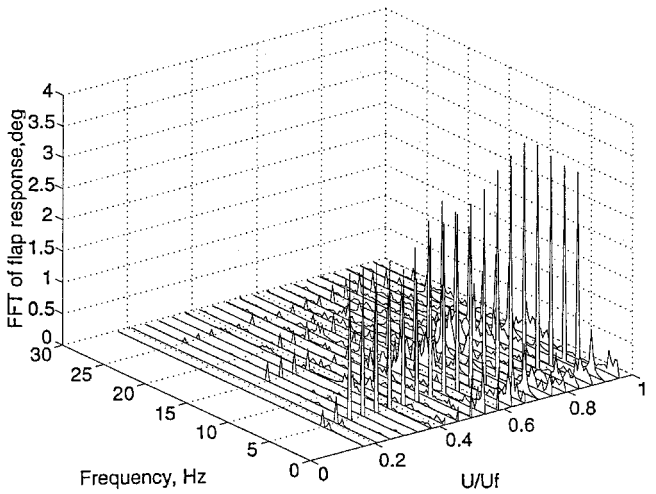

b) Flap response

Fig. 5 FFT analysis vs nondimensional airspeed for gust excitation frequency, $\omega_g = 5$ Hz.

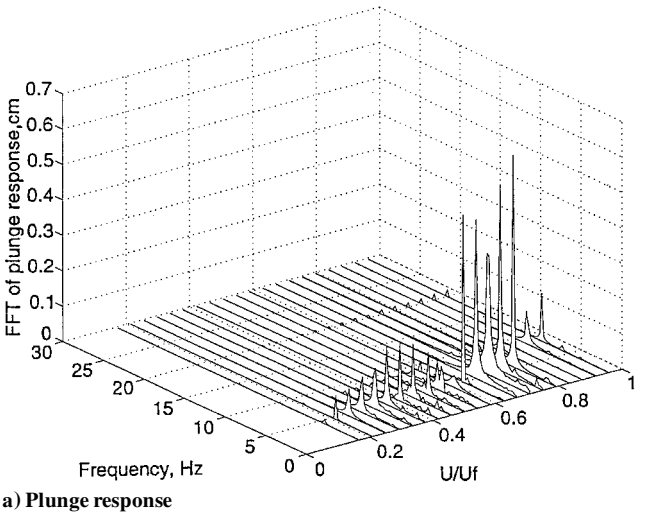

a) Plunge response

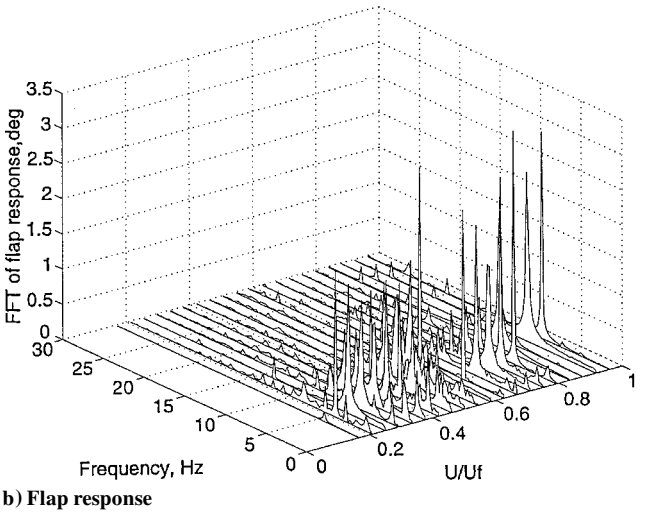

b) Flap response

Fig. 6 FFT analysis vs nondimensional airspeed for gust excitation frequency $\omega_g = 20$ Hz.

in a logical and physically meaningful way using viscous modal damping coefficients (see Ref. 1).

The right-hand side of Eq. (27) forms a vector of aerodynamic forces, $\{F_a\} = \{L, M_\alpha, M_\beta\}^T$. We use Peters's finite state incompressible airloads model for a deformable airfoil[3] and Eq. (13) to determine these aerodynamic forces in a matrix form. They are

$$\{F_a\} = [T]^T\{L_n\} \tag{29}$$

where

$$\{L_n\}/2\pi\rho = bU\lambda_0\{c_1\} - U^2[K][T]\{y\} - bU[C][T]\{\dot{y}\} - b^2[M][T]\{\ddot{y}\} + bU[C]\{w_{gn}\} + b^2[M]\{\dot{w}_{gn}\} \tag{30}$$

then

$$[S_1]\{F_a\} = \lambda_0\{P\} - [K_a]\{y\} - [C_a]\{\dot{y}\} - [M_a]\{\ddot{y}\} + [G_1]\{w_{gn}\} + [G_2]\{\dot{w}_{gn}\}$$

where

$$\{P\}_{3\times1} = 2\pi\rho bU[S_1][T]^T\{c_1\}$$

$$[K_a]_{3\times3} = 2\pi\rho U^2[S_1][T]^T[K][T]$$

$$[C_a]_{3\times3} = 2\pi\rho bU[S_1][T]^T[C][T]$$

$$[M_a]_{3\times3} = 2\pi\rho b^2[S_1][T]^T[M][T]$$

$$[G_1]_{3\times N} = 2\pi\rho bU[S_1][T]^T[C]$$

$$[G_2]_{3\times N} = 2\pi\rho b^2[S_1][T]^T[M]$$

$$\{c_1\}_{N\times1} = \left\{1, -\tfrac{1}{2}, 0, 0, 0, \ldots, 0\right\}^T$$

For matrices $[S_1]$, $[T]$, $[K]$, $[C]$, and $[M]$, see Ref. 3.

Equation (18) gives relationships for λ_n. Unfortunately, λ_0 cannot be determined from Eq.(18). One additional relation is needed that relates λ_0 to λ_n. An approximate λ_0 is determined by

$$\lambda_0 \approx \frac{1}{2}\sum_{n=1}^{N} b_n\lambda_n \tag{31}$$

The closed-form expressions for the b_n are given in Appendix C of Ref. 8.

Collecting Eqs. (18) and (31) gives an inflow matrix equation. It is

$$[A]\{\dot{\lambda}\} + (U/b)\{\lambda\} = [B_1]\{\ddot{y}\} + (U/b)[B_2]\{\dot{y}\} + [B_g]\{\dot{w}_{gn}\} \tag{32}$$

where the matrix $[A]$ is given in Ref. 8 and

$$[B_1]_{N\times3} = \{c_2\}\{s_2\}^T[T], \qquad [B_2]_{N\times3} = \{c_2\}\{s_3\}^T[T]$$

$$[B_g]_{N\times N} = \{c_2\}\{s_2\}^T, \qquad \{c_2\}_{N\times1} = \left\{2, 1, \tfrac{2}{3}, \ldots, 2/N\right\}^T$$

$$\{s_2\}^T_{1\times N} = \left\{1, \tfrac{1}{2}, 0, 0, 0, \ldots, 0\right\}^T$$

$$\{s_3\}^T_{1\times N} = \{0, 1, 2, 3, \ldots, n-1\}^T$$

Equation (32) is basically an equation for the time evolution of vortex transport in the wake of the airfoil. Combining Eqs. (27–32) and defining $X_e = \{\dot{y}, y, \lambda\}^T$, we obtain a set of state-space equations with six structural states and N inflow states. These equations are

$$\dot{X}_e = A_e X_e + B_e \tag{33}$$

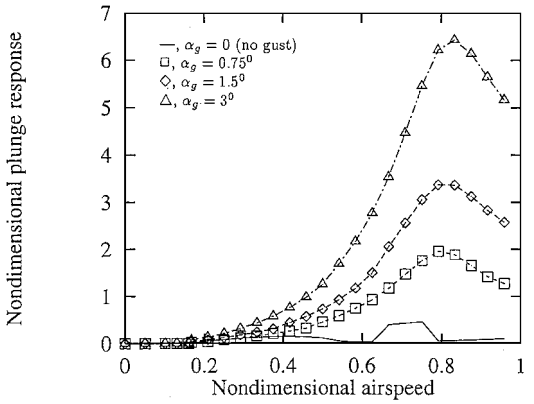

a) Plunge response

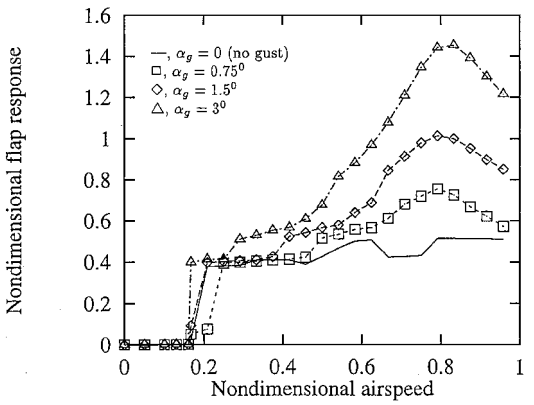

b) Flap response

Fig. 7 Nondimensional structural response vs nondimensional airspeed for gust excitation frequency $\omega_g = 5$ Hz and different gust strengths.

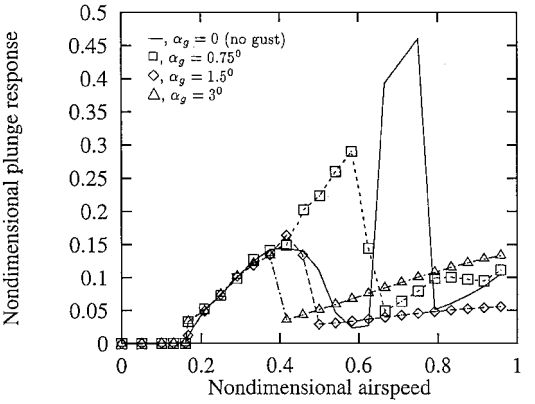

a) Plunge response

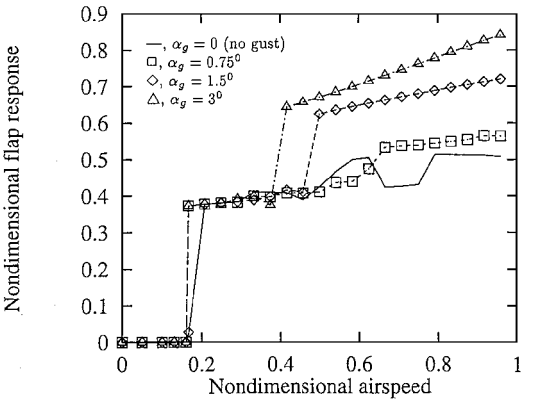

b) Flap response

Fig. 8 Nondimensional structural response vs nondimensional airspeed for gust excitation frequency $\omega_g = 11$ Hz and different gust strengths.

where

$$A_e = \begin{bmatrix} M_e & C_e & 0 \\ 0 & M_e & 0 \\ -B_1 & -(U/b)B_2 & A \end{bmatrix}^{-1} \begin{bmatrix} 0 & -K_e & B_n \\ M_e & 0 & 0 \\ 0 & 0 & -(U/b)I \end{bmatrix}$$

$$B_e = \begin{bmatrix} M_e & C_e & 0 \\ 0 & M_e & 0 \\ -B_1 & -(U/b)B_2 & A \end{bmatrix}^{-1} \times \left(\begin{Bmatrix} 0 \\ -M_\beta \\ 0 \end{Bmatrix} + [G_{e1}]\{w_{gn}\} + [G_{e2}]\{\dot{w}_{gn}\} \right)$$

where submatrices M_e, K_e, and C_e are the equivalent mass, stiffness, and damping matrices comprising structural and aerodynamic components $M_e = [M_s] + [M_a]$, $C_e = [C_s] + [C_a]$, $K_e = [K_s] + [K_a]$ and the submatrix B_n is determined by

$$\lambda_0\{P\} = \left(\frac{1}{2} \sum_{n=1}^{N} b_n \lambda_n \right) \{P\} = B_n\{P\}$$

The matrices $[G_{e1}]$ and $[G_{e2}]$ are given by

$$[G_{e1}] = \begin{bmatrix} |G_1|_{3\times N} \\ |0|_{3\times N} \\ |0|_{N\times N} \end{bmatrix}_{(N+6)\times N}$$

$$[G_{e2}] = \begin{bmatrix} |G_2|_{3\times N} \\ |0|_{3\times N} \\ |B_g|_{N\times N} \end{bmatrix}_{(N+6)\times N}$$

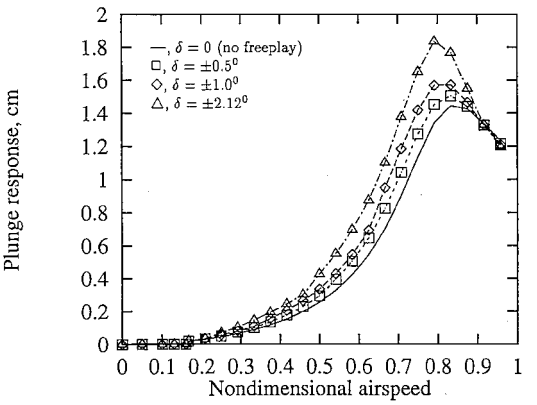

a) Plunge response

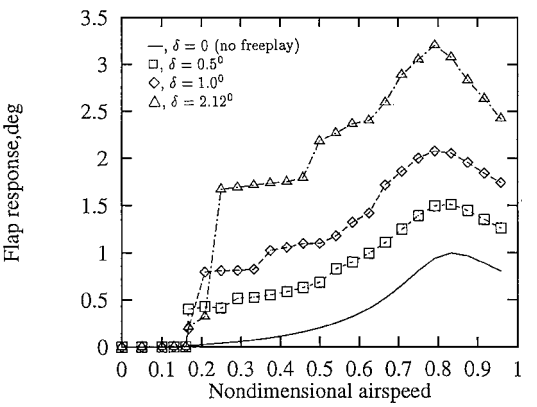

b) Flap response

Fig. 9 Structural response vs nondimensional airspeed for gust excitation frequency $\omega_g = 5$ Hz and different freeplay gaps.

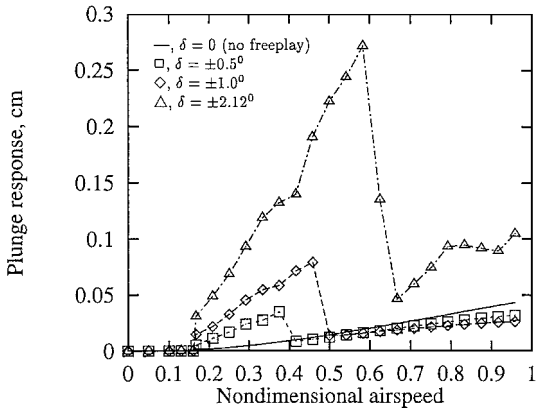

a) Plunge response

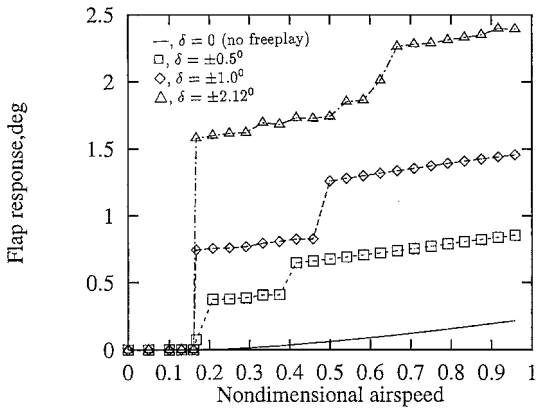

b) Flap response

Fig. 10 Structural response vs nondimensional airspeed for gust excitation frequency ω_g = 11 Hz and different freeplay gaps.

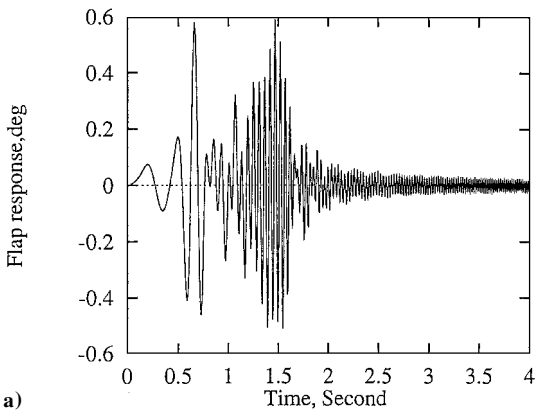

a)

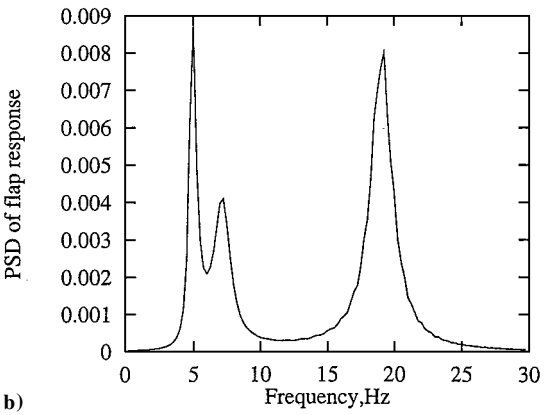

b)

Fig. 11 Linear system at U = 18 m/s or U/U_f = 0.75 a) time response to frequency sweep gust and b) PSD analysis.

Numerical Results and Discussion

The parameters of the numerical model come from the experimental model previously described in Ref. 1. The nominal values for the inertial, stiffness, and damping parameters of the experimental structural system were measured. A summary of the system parameters is given in the Appendix. A comparison of the structural natural frequencies for the numerical and experimental systems is given in Table 1.

The theoretical lateral gust velocity amplitude w_{g0} is 0.75 deg (for the basic case), for a single harmonic gust load.

Table 1 Natural frequencies

Frequency	Numerical	Experimental	% Difference
ω_α(coupled)	7.83 Hz	7.75 Hz	1
ω_β(coupled)	19.2 Hz	19.5 Hz	1.5
ω_h(coupled)	4.34 Hz	4.3 Hz	0.9

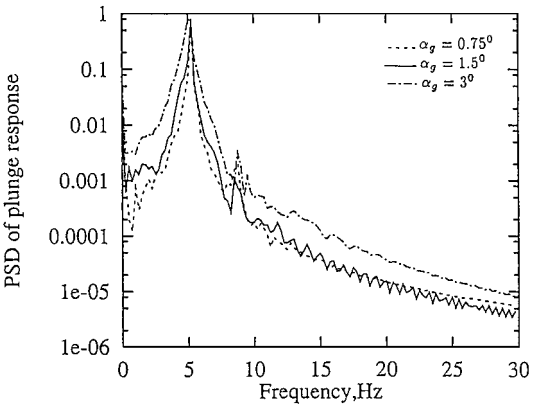

a) Plunge response

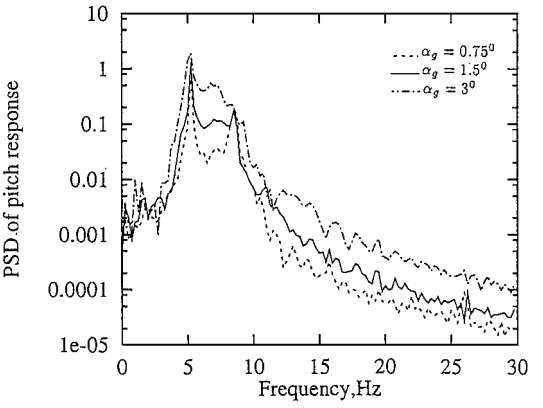

b) Pitch response

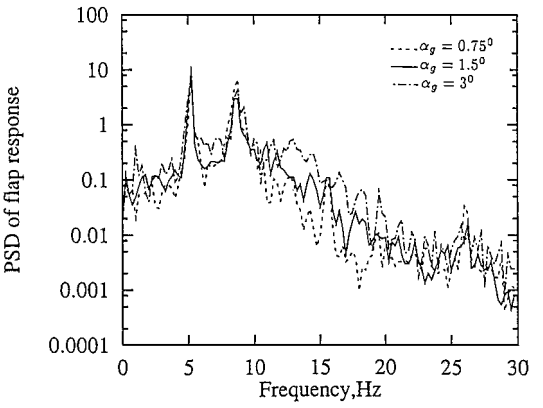

c) Flap response

Fig. 12 Average PSD analysis of structural response for U = 18 m/s or U/U_f = 0.77, δ = ± 2.21 deg, and different gust strengths.

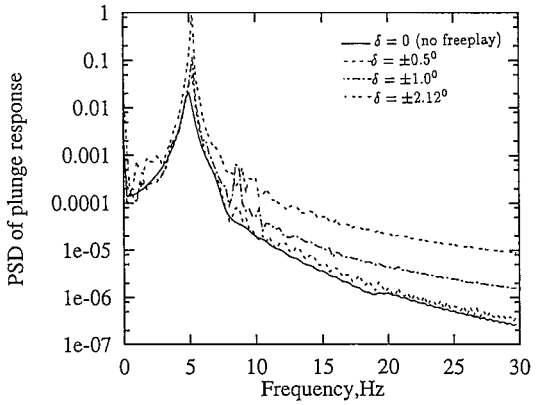

a) Plunge response

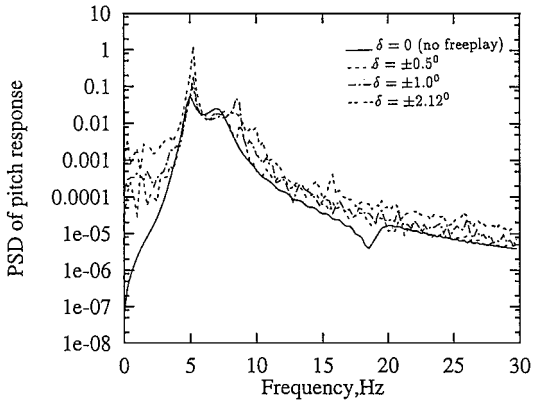

b) Pitch response

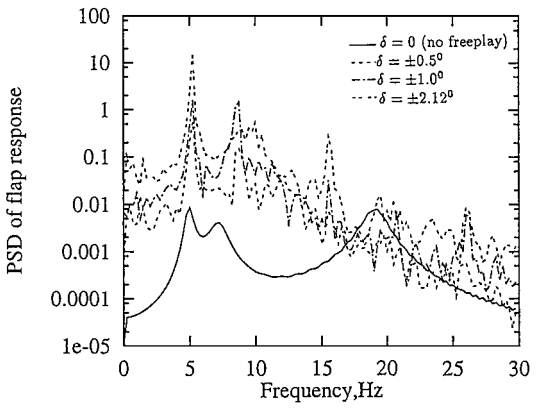

c) Flap response

Fig. 13 Average PSD analysis of structural response for $U = 18$ m/s or $U/U_f = 0.77$, $\alpha_g = 0.75$ deg, and different freeplay gaps and strengths.

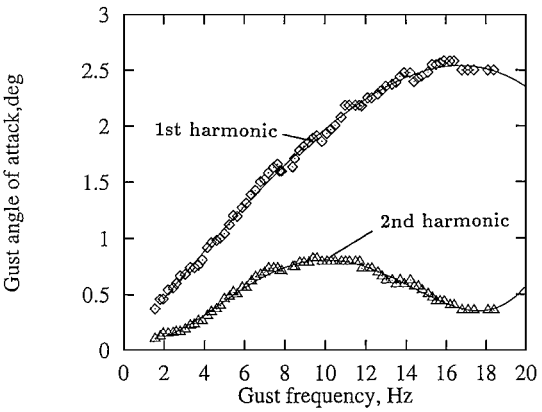

Fig. 14 Gust load vs gust frequency for $U = 15$ m/s or $U/U_f = 0.625$.

When the freeplay gap is zero and the gust excitation is removed, a linear self-excited aeroelastic model is obtained. For the linear system as given by Eq. (33), the structural nonlinearity and gust excitation term B_e are first set to zero to determine the classical linear flutter results. The eigenvalues of the A_e determine the stability of the system. When the real part of any one eigenvalue becomes positive, the entire system becomes unstable. For Eq. (33), we use the augmented closed-form to calculate the coefficients b_i. The number of inflow states is taken as $N = 10$ and the expansion index $n = 10$ (see Ref. 3). The computation used double precision arithmetic. The flutter velocity is equal to $U_f = 24$ m/s, and the corresponding flutter oscillation frequency is $\omega_f = 35.86$ rad/s (5.71 Hz).

Nonlinear Response to Single Harmonic Gust Load

We have used a standard Runge–Kutta algorithm in conjunction with the Peters's aerodynamic model [Eq. (33)] for time integration of the nonlinear equations. Before we determine the gust response of the typical airfoil section with control surface freeplay, the nonlinear behavior without gust load ($w_g = 0$) has been calculated. The initial condition is defined to have only a plunge disturbance with amplitude 0.1 cm, $h(0) = 0.1$ cm.

As a typical experimental case, a freeplay region of ±2.12 deg is considered ($\delta = 2.12$ deg). The model was placed in the wind tunnel such that the control surface was resting at one edge of the

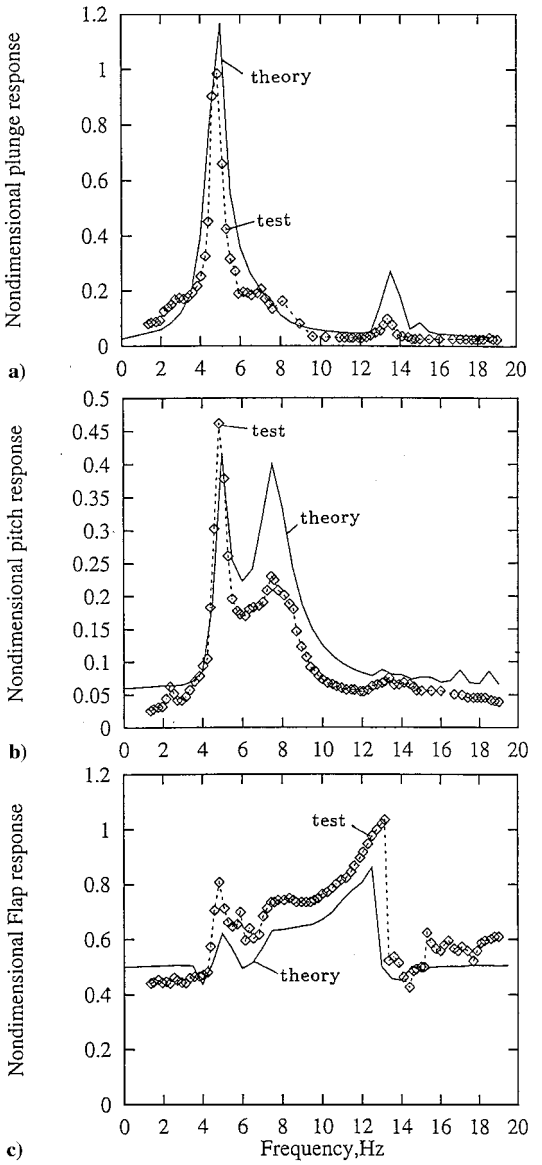

Fig. 15 Nondimensional structural response vs gust excitation frequency for $U = 15$ m/s or $U/U_f = 0.625$: a) plunge response, b) pitch response, and c) flap response.

freeplay region. As the airflow in the tunnel was increased, this non-zero initial condition in the flap served to excite the system, causing the wing to settle into a steady-state limit cycle. The airflow was slowly increased to a new value and reached a new steady-state limit. The behavior of the system was examined below the nominal linear flutter speed.

For no gust load, the nonlinear behavior is shown in Figs. 2 and 3. Figure 2 shows a nondimensional limit cycle amplitude ($h_{\text{rms}}/2\delta$, $\alpha_{\text{rms}}/2\delta$, and $\beta_{\text{rms}}/2\delta$) vs airflow speed ratio (U/U_f). The amplitudes shown are based on rms calculations over one cycle of the numerical steady-state time histories. In Fig. 2, ◇ indicates the plunge motion, and □ and △ indicate the pitch and flap responses, respectively. A fast Fourier transform (FFT) of plunge response and flap response vs frequency and airflow speed ratio is shown in Figs. 3a and 3b, respectively.

Some different types of motion were found from the numerical predictions. For low velocities, $U < 0.18 \times U_f$, an initial disturbance to the model resulted in decaying oscillations that damped to zero fairly quickly.

At $U \approx 0.18 \times U_f$, there is a discrete jump from damped motion to a low-frequency limit cycle oscillation (about 4.6 Hz) that is dominated by the plunge motion DOF as shown in Fig. 3a. Note that the first natural frequency of the linear system dominated by plunge motion is 4.32 Hz. The flap motion is complex, as shown in Fig. 3b. This limit cycle behavior is observed until the airflow speed reaches approximately $0.45 \times U_f$.

In a range between $U = 0.45$ and $0.625 \times U_f$, there is a transition response from lower (about 5 Hz dominated by the plunge motion) to higher (about 9 Hz dominated by the flap motion) frequency oscillations, as shown in Figs. 3.

At $U \approx 0.66 \times U_f$, there is another abrupt change in the system behavior. The high-frequency limit cycle suddenly becomes unstable, and the system is attracted to a stable, low-frequency limit cycle.

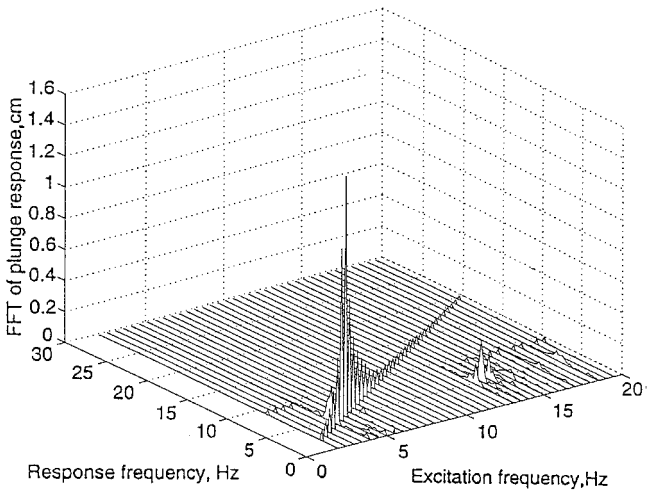

a) Plunge response

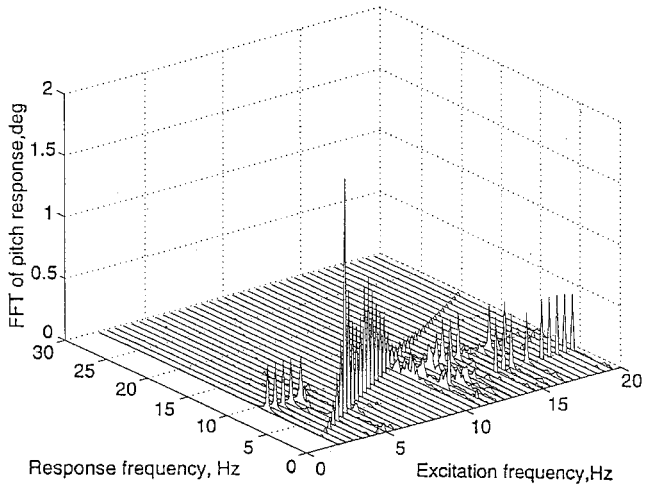

b) Pitch response

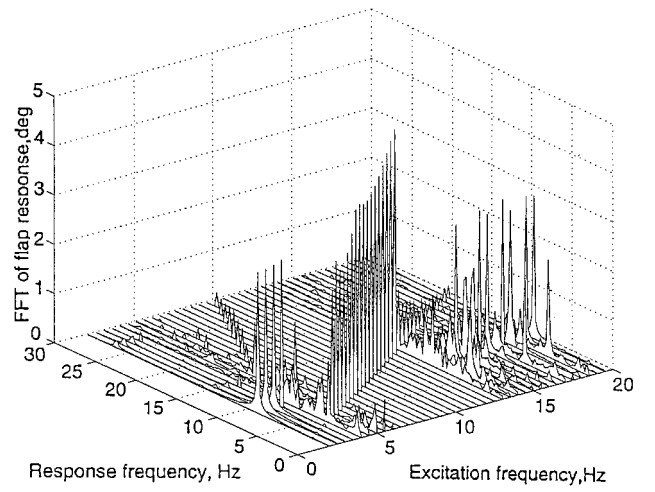

c) Flap response

Fig. 16 FFT analysis vs response frequency for different gust excitation frequency, $U = 15$ m/s or $U/U_f = 0.625$.

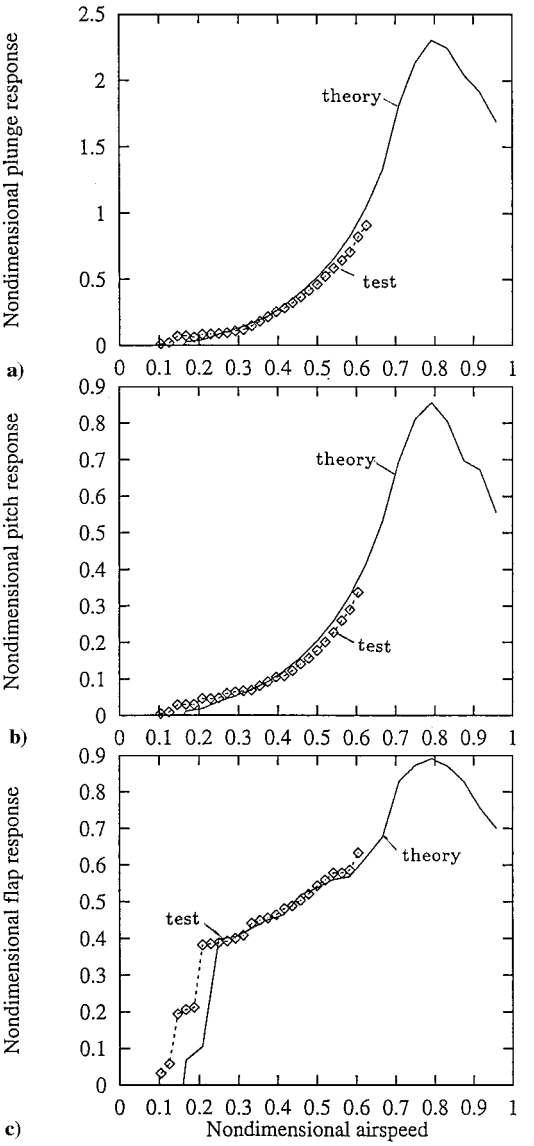

Fig. 17 Nondimensional structural response vs nondimensional airspeed for gust excitation frequency $\omega_g = 5$ Hz: a) plunge response, b) pitch response, and c) flap response.

There is a jump in the plunge amplitude at this point. The oscillation frequency of both plunge and flap is near 5 Hz.

When the velocities $U > 0.75 \times U_f$, a high-frequency limit cycle oscillation (LCO) (about 9.0 Hz) was observed again. Note that the second natural frequency of the linear system dominated by pitch motion is 7.83 Hz. The LCO amplitudes mostly increase as the flow velocity increases for both pitch and flap motions.

Figures 4a–4c show the nondimensional plunge (Fig. 4a), pitch (Fig. 4b), and flap (Fig. 4c) limit cycle amplitude vs airflow speed ratio for several gust excitation frequencies, $\omega_g = 5$, 11, and 20 Hz with no initial disturbance and also for no gust excitation with $h(0) = 0.1$ cm initial plunge disturbance ($\omega_g = 0$). In Figs. 4, □ indicates those responses for $\omega_g = 5$ Hz, and ◇ and △ indicate those for $\omega_g = 11$ and 20 Hz, respectively. The solid line indicates the results for $\omega_g = 0$. For the results of $\omega_g = 5$ Hz, the LCO amplitudes increase as the flow velocity increases up to nondimensional flow velocity 0.8 for plunge, pitch, and flap motions, whereas from 0.8 to 0.96, the LCO amplitudes decrease. The results for $\omega_g = 0$, 11, and 20 Hz are all substantially smaller. From an FFT analysis, the plunge response is almost a single frequency oscillation with $\omega_g = 5$ Hz as shown in Fig. 5a, but a multiple frequency oscillations is seen for the flap motion as shown in Fig. 5b.

Returning to Figs. 4b and 4c, we note again the results for $\omega_g = 11$ and 20 Hz are very similar to those for $\omega_g = 0$. This is because the gust frequency is far away from the system natural frequency and the gust strength ($\alpha_g = 0.75$ deg) is relatively weak. Corresponding to Figs. 4b and 4c, results from an FFT analysis are shown in Figs. 6a and 6b ($\omega_g = 20$ Hz). It is found that the frequency component corresponding to the excitational frequency is not significant for either plunge or flap motion.

Next, we discuss the effects of the gust strength and the freeplay gap of the control surface on the behavior of this nonlinear system.

Figure 7 shows the nondimensional plunge and flap responses vs the nondimensional airspeed for several different gust strengths, $\alpha_g = 0$ (no gust load), 0.75, 1.5, and 3 deg with a gust excitation frequency $\omega_g = 5$ Hz. Generally the results indicate that as the airspeed increases, the LCO amplitude of the structural response increases until the airspeed is near the linear flutter speed. Here the gust excitation frequency is near the plunge natural frequency of the system. However, when the gust frequency is changed to 11 Hz (Fig. 8), the plunge amplitude may decrease as the airspeed increases in the nondimensional airspeed range of 0.66–0.75. Thus, the gust excitation may have a quenching effect on the plunge motion. On the other hand, the amplitude for the flap response increases as the airspeed increases. Here the gust frequency is far away from the first natural frequency of the system and approaches the LCO frequency of this nonlinear system. Note that the response levels in Fig. 8 are generally smaller than those of Fig. 7.

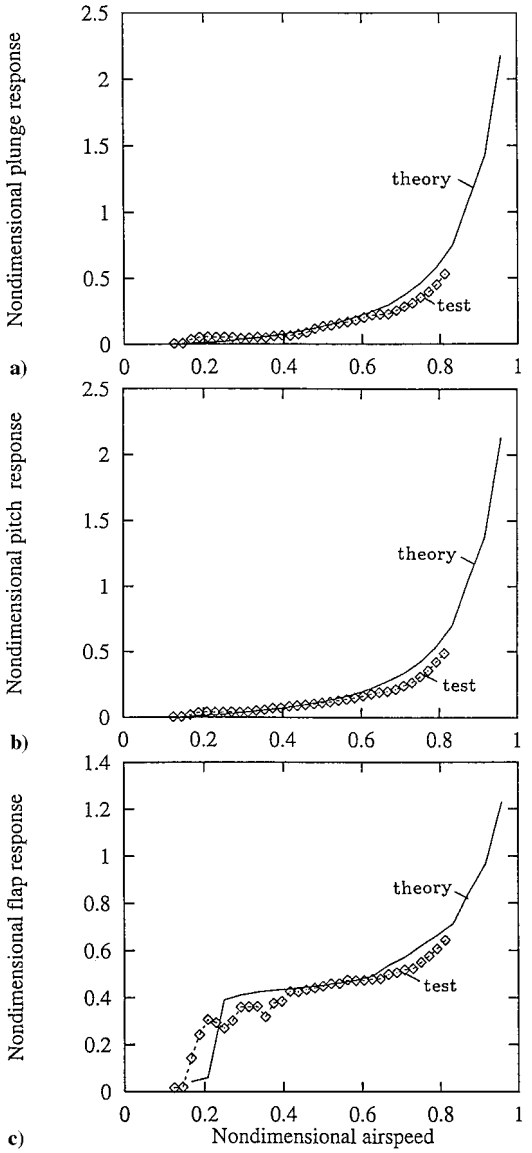

Fig. 18 Nondimensional structural response vs nondimensional airspeed for gust excitation frequency $\omega_g = 6$ Hz: a) plunge response, b) pitch response, and c) flap response.

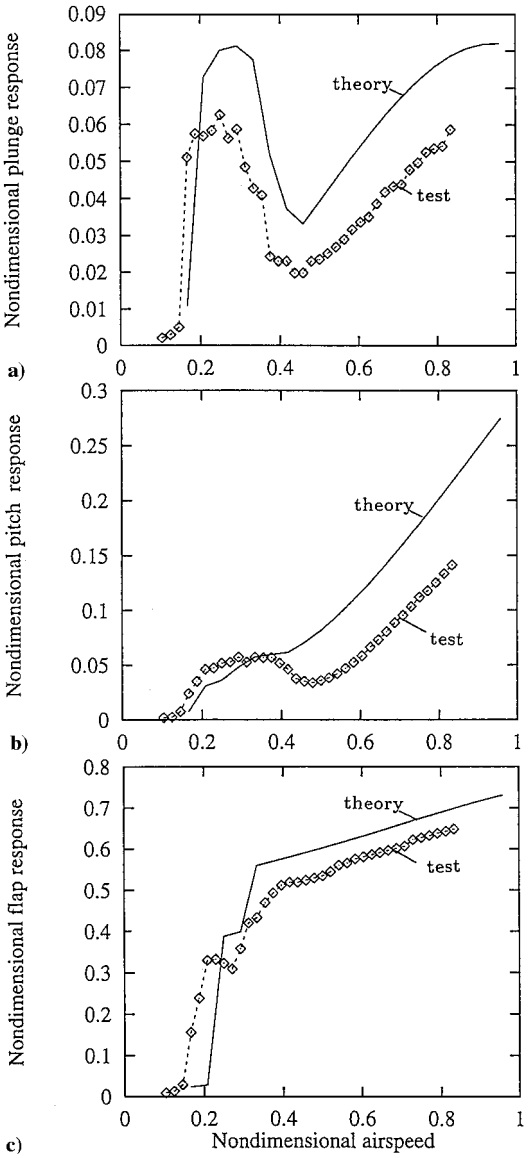

Fig. 19 Nondimensional structural response vs nondimensional airspeed for gust excitation frequency $\omega_g = 10$ Hz: a) plunge response, b) pitch response, and c) flap response.

Figures 9 shows the plunge (Fig. 9a) and flap (Fig. 9b) responses vs the nondimensional airspeed for a gust frequency $\omega_g = 5$ Hz, a gust amplitude $\alpha_g = 0.75$ deg, and several freeplay gaps, $\delta = 0$ deg (no freeplay), ± 0.5, ± 1.0, and ± 2.12 deg. The results show that the amplitude of the structural response increases as the freeplay increases. Results for the gust frequency $\omega_g = 11$ Hz are shown in Figs. 10a and 10b. Note that in Figs. 10 the plunge response is much smaller than for Figs. 9.

From nondimensional analysis of the equations of motion one may show that when the responses h, α, and β and the excitation α_g are normalized by the freeplay δ the results are universal, that is, the normalized results are the same for any δ.

Nonlinear Response to a Sweep Frequency Gust Load

The basic theoretical lateral gust velocity amplitude w_{g0} is 0.75 deg for a continuous linear frequency sweep gust load. The minimum and maximum frequencies are 0 and 40 Hz, and the sweep duration T is 2.4 s. The initial conditions are set to zero for all time simulations.

Linear system results are examined. Figures 11 shows a time history (Fig. 11a) and a power spectral density (PSD) analysis (Fig. 11b) for the flap response due to a sweep frequency gust at $U =$ 18 m/s. From Fig. 11b, we find the three resonant frequencies are 5.0, 7.8, and 19.3 Hz, which are very close to the system natural frequencies. Because of an increased aerodynamic stiffness, the first aeroelastic natural frequency is higher than the first structural natural frequency (4.34 Hz) in vacuo.

To depict concisely the nonlinear response to the sweep frequency gust, an average PSD analysis can be used. Here, 40 PSD realizations are taken. More than 40 PSD realizations do not change the averaged results significantly.

Figure 12 shows the averaged PSD for an airspeed of $U =$ 18 m/s and several different gust strengths, $\alpha_g = 0.75$, 1.5, and 3 deg. The freeplay is $\delta = \pm 2.12$ deg. For the larger gust strengths, $\alpha_g =$ 1.5 and 3 deg, the structural responses have a maximum peak value at $\omega = 5.2$ Hz. The response motion is dominated by the flap motion; compare Fig. 12c with Figs. 12a and 12b at $\omega = 5.2$ Hz. As shown

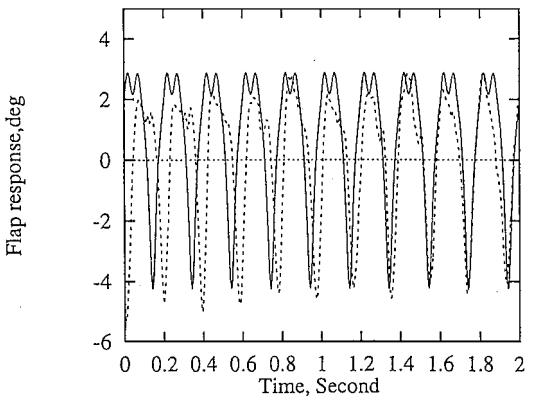

a) Time history

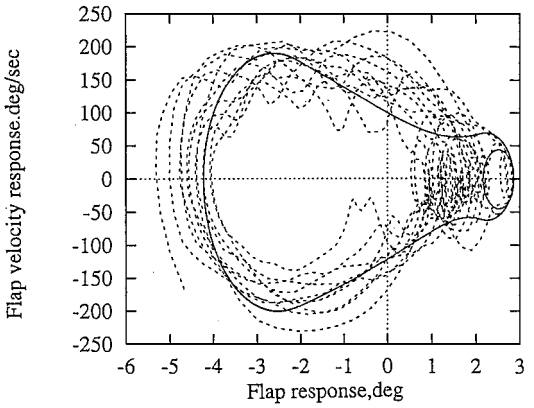

b) Phase plane plot

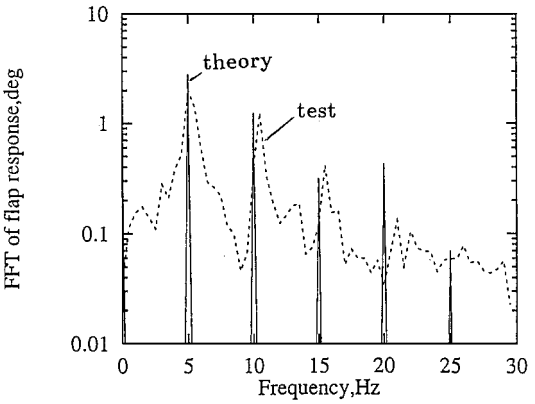

c) FFT analysis

Fig. 20 Structural flap response behavior for gust excitation frequency $\omega_g = 5$ Hz and $U = 12$ m/s or $U/U_f = 0.5$.

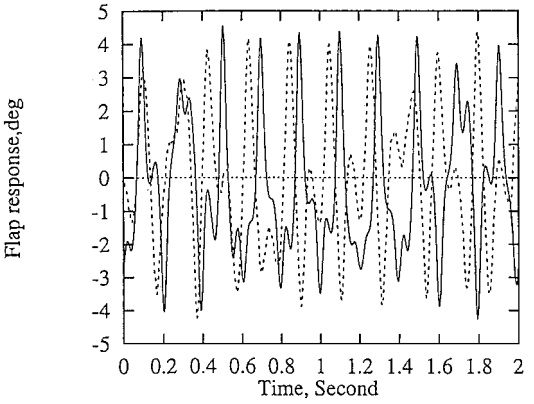

a) Time history

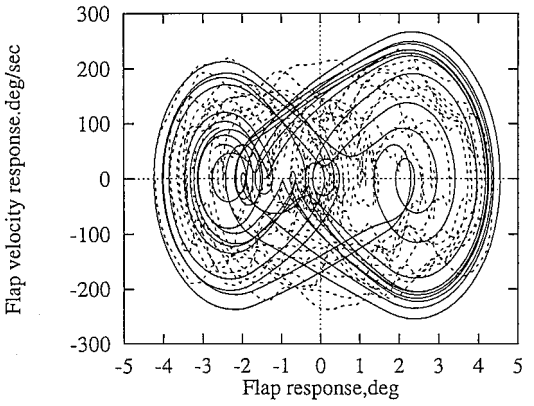

b) Phase plane plot

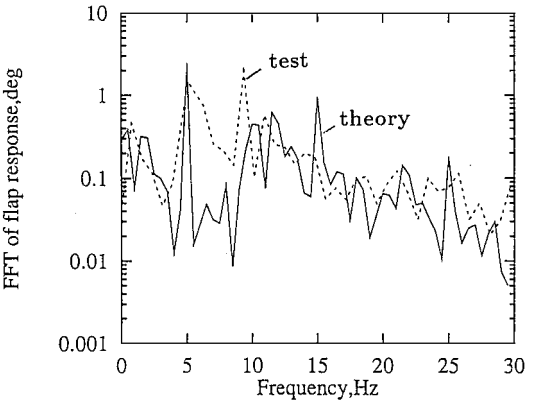

c) FFT analysis

Fig. 21 Structural flap response behavior for gust excitation frequency $\omega_g = 5$ Hz and $U = 14$ m/s or $U/U_f = 0.58$.

in Fig. 12c, the flap structural response component at $\omega = 8.5$ Hz is also not small.

Figure 13 shows the averaged PSD for an airspeed of $U = 18$ m/s and several different freeplay gaps, $\delta = 0$, ± 0.5, ± 1.0, and ± 2.12 deg. The gust strength is $\alpha_g = 0.75$ deg. As shown in Fig. 13, the maximum plunge, pitch, and flap peak amplitudes increase as the freeplay gap increases, respectively. When freeplay gap approaches zero, the structural responses are much smaller, especially for the flap amplitude. Similar to the results of Fig. 12, the structural responses have a maximum peak value at $\omega = 5.2$ Hz, and the motion is dominated by plunge.

Experimental Results and Discussion

A three-DOF aeroelastic typical section with control surface freeplay is modeled experimentally. The experimental model, measurement system, and data acquisition are described in Ref. 1.

The periodic gust load was created by placing an RSC behind an airfoil upstream of the airfoil model. The gust generator configuration in the wind tunnel had two airfoils or vanes and two rotating slotted cylinders. The distance between these vanes was 0.3 m. For details of the gust generator design, see Ref. 9.

All gust response tests of the two-dimensional wing model with control surface freeplay were performed in the Duke University low-speed wind tunnel.

Figure 14 shows a typical measured gust strength α_g vs gust excitation frequency (hertz) for the flow velocity $U = 15$ m/s. In Fig. 14, ◇ indicates the measured first harmonic component and △ indicates the second harmonic component. The solid line indicated the least-square curve fitting from the experimental data. The gust strength varies with the gust frequency and is not a pure sinusoid. The second harmonic component should be not neglected. In the theoretical calculations we use the measured experimental gust load for comparison with the experimental results.

Figure 15 shows the correlation between the theoretical and experimental results for the nondimensional plunge, pitch, and flap responses vs gust excitation frequency at the flow velocity $U = 15$ m/s. The correlation is reasonable except for the plunge response near $\omega = 13.5$ Hz and the pitch response near $\omega = 7.8$ Hz. Corresponding to Fig. 15, a theoretical FFT analysis of plunge, pitch, and flap responses vs response frequency and gust excitation frequency is shown in Figs. 16a, 16b, and 16c, respectively. As shown in Fig. 16a, the dominant plunge response frequency is nearly equal to the gust frequency except near an excitation frequency of 13.5 Hz, where the 5-Hz frequency component is most important for the response. The latter is the original (no gust) LCO frequency of the nonlinear system (the LCO frequency is about 5 or 9 Hz). As shown in Fig. 16c, the dominant flap response frequency is consistent with the gust frequency when the latter is in the range of $\omega = 5$–13 Hz. For gust frequencies lower than 5 Hz and higher than 14 Hz, the flap response is dominated by the response component with a frequency of about 9 Hz, which is the original LCO frequency of the nonlinear system. A similar result for the pitch response is shown in Fig. 16b. The responses between 5 and 10 Hz are dominated by the pitch motion, and the response frequency is nearly equal to the gust frequency. Beyond these excitation frequencies, the responses are dominated by the flap or plunge motions.

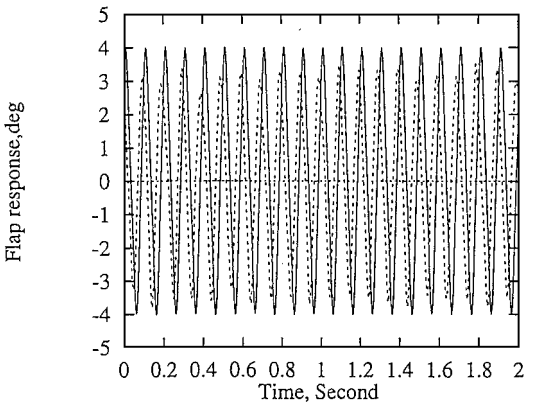

a) Time history

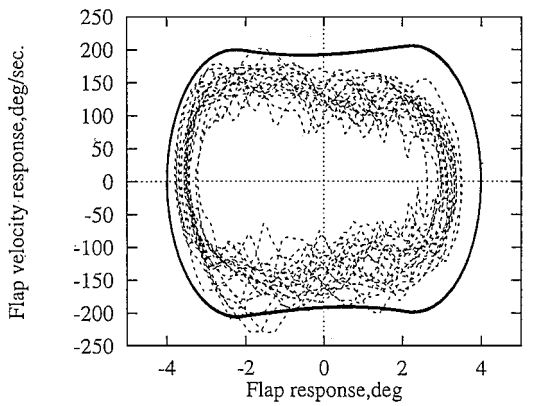

b) Phase plane plot

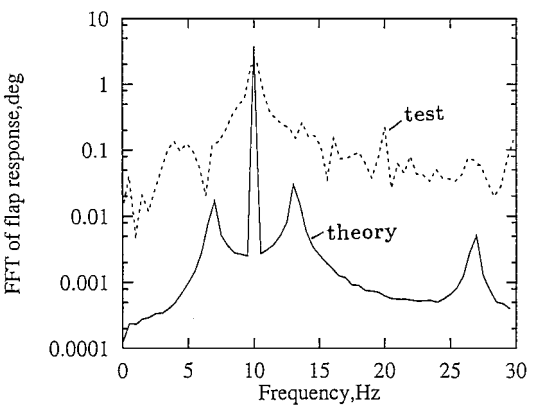

c) FFT analysis

Fig. 22 Structural flap response behavior for gust excitation frequency $\omega_g = 10$ Hz and $U = 12$ m/s or $U/U_f = 0.5$.

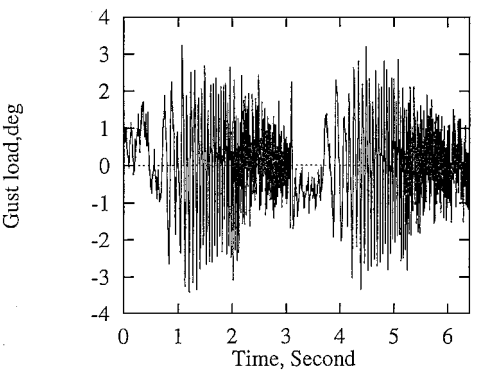

a) Measured data

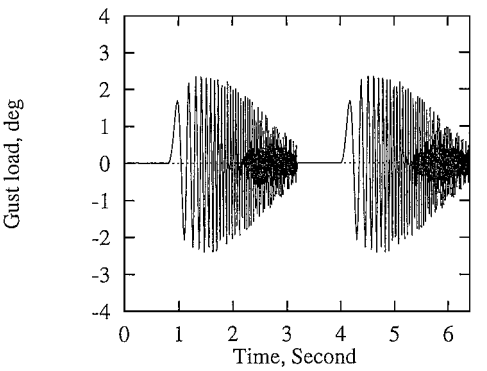

b) Numerical simulation

Fig. 23 Continuous linear frequency sweep gust load for $U = 12$ m/s or $U/U_f = 0.5$.

In an effort to explain the differences between theory and experiment in Fig. 15, different values of structural damping were considered in the theoretical model. However, the theoretical results are not sensitive to this parameter.

Figures 17–19 show the correlation between the theoretical and experimental results for the nondimensional plunge (Figs. 17a–19a), pitch (Figs. 17b–19b), and flap (Figs. 17c–19c) responses vs nondimensional airspeed plunge for the gust frequencies $\omega =$ 5, 6, and 10 Hz, respectively. The solid line indicates the results from theory and the symbol ◇ from the experiment. As seen from Figs. 17 ($\omega =$ 5 Hz) and 18 ($\omega = 6$ Hz), the agreement between the theory and experiment is good. The measured response signal is strong and has very good signal to noise ratio. For $\omega = 10$ Hz, [Fig. 19], the plunge and pitch responses have poorer theoretical/experimental correlation, and this may be because of the weaker measured response signals. However, the correlation for the flap response is reasonable.

Figure 20 shows an example of the flap response time history and corresponding phase plane plot and FFT analysis for $\omega = 5$ Hz and $U = 12$ m/s. The solid and dashed lines indicate the theoretical and experimental results, respectively. The theoretical results have a periodic behavior; however, the experimental results look like a narrow-band random or chaotic oscillation. The agreement of the basic frequency and rms amplitude between theory and experiment is good. Following Fig. 20, when the flow velocity increases to $U = 14$ m/s, we find the amplitude increases and a chaotic oscillation occurs for both the theoretical and experimental results as shown in Fig. 21. The theoretical results have one dominant frequency component at $\omega = 5$ Hz, but the experimental results have two dominant frequency components at $\omega = 5$ and 9 Hz, as shown in Fig. 21c.

Figure 22 shows the flap response time history and corresponding phase plane plot and FFT analysis for $\omega = 10$ Hz and $U = 12$ m/s. The solid and dashed lines indicate the theoretical and experimental results, respectively. A result similar to Fig. 20 is also found. The theoretical results have a periodic behavior, and the experimental results look like a narrow-band random or chaotic oscillation. The difference in the LCO behavior between theory and experiment may be due to the turbulence caused by the interfering wake vortex of the gust generator in the experimental data. Because the turbulence is not strong, the theoretical/experimental quantitative agreement still remains good when comparing averaged (rms) data.

Figure 23a shows a measured continuous linear frequency sweep gust load (angle of attack) for $U = 12$ m/s. The gust strength is not constant with time as shown in Eq. (23) and in Figs. 11–13. For the measured lateral gust, the minimum and maximum frequencies are 0 and 40 Hz, and the sweep duration T is 2.4 s. Note that the measured lateral gust has about a 0.8-s time delay, that is, the restarting time of the dc motor for each repeated process. This is due to the rotational inertia of the dc motor. For convenient application, a formula based on an experimental gust load is constructed:

$$w_g(t) = \bar{w}_{gs}(t)\sin\{\omega_1 + [(\omega_2 - \omega_1)/2T]t\}t \tag{34}$$

where $w_{gs}(t)$ (second) is given by

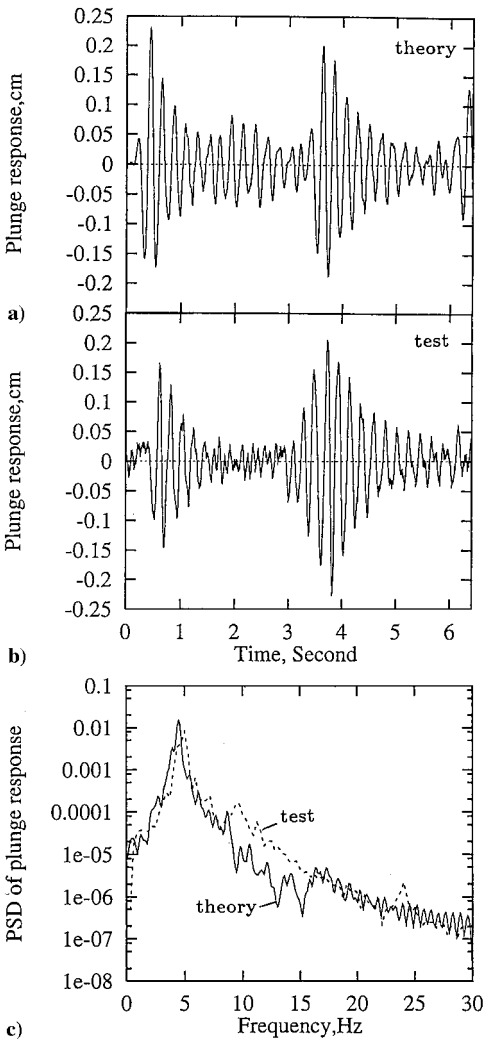

Fig. 24 Structural plunge response behavior under a continuous linear frequency sweep gust load for $U = 12$ m/s or $U/U_f = 0.5$: a) theoretical time history, b) experimental time history, and c) PSD analysis.

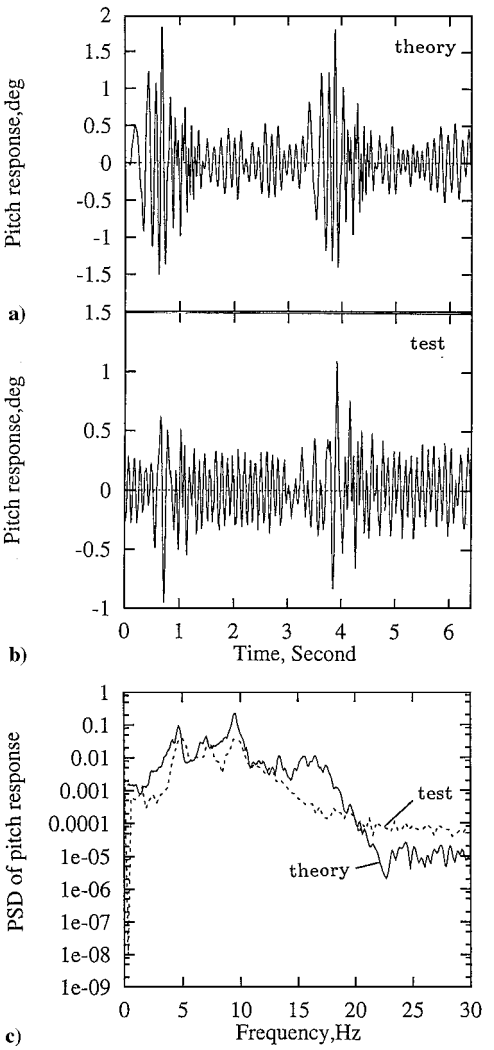

Fig. 25 Structural pitch response behavior under a continuous linear frequency sweep gust load for $U = 12$ m/s or $U/U_f = 0.5$: a) theoretical time history, b) experimental time history, and c) PSD analysis.

$$w_{gs}(t) = \begin{cases} 0, & 0 < t < 0.8 \\ \sum_{i=0}^{4} c_i t^i, & 0.8 \le t \le 3.2 \end{cases} \quad (35)$$

where $c_0, \ldots, c_4$ are determined by the least-square curve-fitting method from the experimental data.

Using Eqs. (34) and (35), the theoretical and experimental results of plunge, pitch, and flap responses are shown in Figs. 24–26 for the flow velocity $U = 12$ m/s, respectively. There are 10 sweep periods in 32 s, and the total sampling length is 51,200 points for the experimental data. Figures 24a–26a indicate the theoretical and Figs. 24b–26b the experimental results. Figures 24c–26c indicate a corresponding PSD plot of both theoretical (solid line) and experimental (dashed line) results for an average over 10 sweep periods.

As shown in Figs. 24a–26a and 24b–26b, the theoretical and experimental response behavior and amplitude are very close. As shown in Figs. 24c–26c of the PSD plot, there is a difference in the dominant frequency. The peak frequency is 4.85 Hz for the theory and 5 Hz for the experiment, as shown in Fig. 24c. This means the response is dominated by the plunge motion. As shown in Fig. 25c, there are three peak frequencies. They are 4.85, 7.6, and 9.25 Hz for the theory and 5, 8, and 9.5 Hz for the experiment. Note that 7.6 and 8 Hz are close to the pitch natural frequency of this linear system and 5 and 9 Hz are close to the LCO frequencies of this nonlinear system. The pitch response includes three frequency components and is very complex. As shown in Fig. 26c, there is a dominant peak frequency for the flap motion. It is 9 Hz for the theory and 9.5 Hz for the experiment. This means the response is dominated by the flap motion. From Figs. 24–26, it is found the theoretical and experimental correlation is reasonably good.

Further investigation of the present method should be considered including more general representations of atmospheric turbulence, rather than the special periodic gust that we used here. Also an investigation of active control for these responses would be of interest. Clark et al.[10] and Vipperman et al.[11] have studied active control of self-excitations for this system.

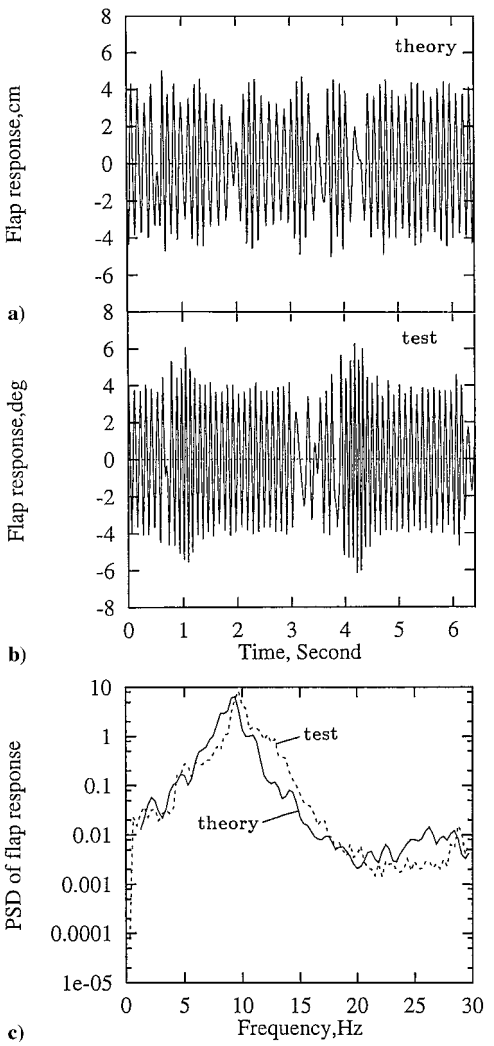

Fig. 26 Structural flap response behavior under a continuous linear frequency sweep gust load for $U = 12$ m/s or $U/U_f = 0.5$: a) theoretical time history, b) experimental time history, and c) PSD analysis.

Conclusion

A nonlinear response analysis of a typical airfoil section with control surface freeplay excited by periodic and continuous linear frequency sweep gust loads in low subsonic flow has been presented. The theoretical approach uses Peters's finite state airloads model.[3] An experiment using an RSC gust exciter was also conducted. Results for a single harmonic gust and a continuous frequency sweep gust (mimicking a random gust) have been computed and measured over a range of lower flow velocities ($U < U_f$) where U_f is the nominal linear flutter velocity in the absence of freeplay. It was shown that the effects of freeplay structural nonlinearity on the dynamic aeroelastic behavior are significant. A theoretical and experimental chaotic response phenomenon for the nonlinear structural model was observed for the single harmonic gust excitation. These results complement our earlier theoretical and experimental studies[1,4,5] of LCO due to self-excited flutter.

The fair to good quantitative agreement between theory and experiment verifies that the present method has reasonable accuracy and good computational efficiency for nonlinear gust response analysis in the time domain.

Appendix: Model Parameters

Table A1 Model parameters

Parameter	Value
Geometry	
Chord	0.254 m
Span	0.52 m
Semichord b	0.127
Elastic axis a with respect to b	−0.5
Hinge line c with respect to b	0.5
Mass parameters	
Mass of wing	0.713 kg
Mass of aileron	0.18597 kg
Mass/length of wing aileron	1.73 kg
Mass of support blocks	0.47485 × 2 kg
Inertial	
x_α	0.331
x_β	0.0188
I_α (per span)	0.087 kg · m
I_β (per span)	0.000254 kg · m
r_α	0.821
r_β	0.11397
Stiffness	
K_α (per span)	1460 1/s^2
K_β (per span)	151 1/s^2
K_h (per span)	1593 1/s^2
Damping	
ζ_α (half-power)	0.0175
ζ_β (half-power)	0.006
ζ_h (half-power)	0.0033

Acknowledgments

This work was supported under U.S. Air Force Office of Scientific Research Grant Limit Cycle Oscillations and Nonlinear Aeroelastic Wing Response and NASA Langley Research Center Grant Flutter of Wing and Control Surface with Freeplay. Brian Sanders and Donald Keller are the respective Grant Monitors. The authors would also like to thank David Peters for his very helpful discussion of his work that has been the basis for our extension of his approach. They would also like to acknowledge useful discussions with Dale Pitt.

References

[1]Conner, M. D., Tang, D. M., Dowell, E. H., and Virgin, L. N., "Nonlinear Behavior of a Typical Airfoil Section with Control Surface Freeplay: A Numerical and Experimental Study," *Journal of Fluids and Structures*, Vol. 11, No. 1, 1997, pp. 89–109.

[2]Edwards, J. W., Ashley, H., and Breakwell, J. V., "Unsteady Aerodynamic Modeling for Arbitrary Motions," *AIAA Journal*, Vol. 17, No. 4, 1979, pp. 365–374.

[3]Peters, D. A., "Finite-State Airloads for Deformable Airfoils on Fixed and Rotating Wings," Symposium on Aeroelasticity and Fluid/Structure Interaction, American Society of Mechanical Engineers, Winter Annual Meeting, Nov. 1994, rev. 3, May 1996.

[4]Tang, D. M., Conner, M. D., and Dowell, E. H., "Reduced-Order Aerodynamic Model and Its Applications to a Nonlinear Aeroelastic System," *Journal of Aircraft*, Vol. 35, No. 2, 1998, pp. 332–338.

[5]Pitt, D. M., "Further Physical Explanations of Free Play Effects on Chaotic Flutter Response of All-Movable Control Surfaces," Second International Conf. on Nonlinear Problems in Aviation and Aerospace, April 1998.

[6]"Military Specification Airplane Strength and Rigidity Vibration, Flutter, and Divergence," MILA8870B(AS), 20 May 1987.

[7]Dowell, E. H., Crawley, E. F., Curtiss, H. C., Jr., Peters, D. A., Scanlan, R. H., and Sisto, F., *A Modern Course in Aeroelasticity*, 3rd ed., Sijthoff and Noordhoff, Alphen ann den Rijn, The Netherlands, 1995, pp. 193–227.

[8]Peters, D. A., and Cao, W. M., "Finite State Induced Flow Models, Part I: Two-Dimensional Thin Airfoil," *Journal of Aircraft*, Vol. 32, No. 2, 1995, pp. 313–322.

[9]Tang, D. M., Cizmas, P. G. A., and Dowell, E. H., "Experiments and Analysis for a Gust Generator in a Wind Tunnel," *Journal of Aircraft* , Vol. 33, No. 1, 1996, pp. 139–148.

[10]Clark, R. L., Dowell, E. H., and Frampton, K. D., "Control of a Three-Degree-of-Freedom Airfoil with Limit Cycle Behavior," *Journal of Aircraft*, Vol. 37, No. 3, 2000, pp. 533–536.

[11]Vipperman, J. S., Clark, R. L., Conner, M., and Dowell, E. H., "Experimental Active Control of a Typical Section Using a Trailing Edge Flap," *Journal of Aircraft*, Vol. 35, No. 2, 1998, pp. 224–229.

A. N. Palazotto
Associate Editor